CrystEngComm

ROYAL SOCIETY OF CHEMISTRY

PAPER

View Article Online
View Journal | View Issue

Check for updates

Cite this: *CrystEngComm*, 2024, **26**, 4541

Liquid-phase intermediated chemical vapor deposition for ternary compositional 1D van der Waals material $Nb_2Pd_3Se_8$†

Sang Hoon Lee,‡[a] Byung Joo Jeong,‡[a] Kyung Hwan Choi,[b] Jiho Jeon,[b] Bom Lee,[a] Sooheon Cho,[a] Dahoon Kim,[a] Gutema Teshome Gudena,[c] Daba Deme Megersa,[c] Sang Hyuk Kim,*[a] Hak Ki Yu *[c] and Jae-Young Choi *[abd]

In the case of low-dimensional semiconductor devices, the basic physical properties of materials can be measured through device manufacturing using single crystal synthesis and exfoliation, but for expansion into various application fields, technology that can synthesize the material itself directly on the substrate is needed. For multi-composition low-dimensional semiconductor materials like $Nb_2Pd_3Se_8$, the physical characteristics of constituent elements differ, making direct growth control on a substrate extremely challenging. This study successfully synthesized $Nb_2Pd_3Se_8$ wires using different metal precursors (niobium and palladium) through liquid precursor–intermediated chemical vapor deposition (LPI-CVD). By adjusting the concentration of the liquid precursor and the synthesis temperature, the reproducible growth of $Nb_2Pd_3Se_8$ wires was achieved, ranging in lengths from 2.29 to 15.04 μm. It was confirmed that $PdSe_2$ is initially synthesized at lower temperatures (below 620 °C), and at temperatures above 620 °C, this $PdSe_2$ transforms into $Pd_{17}Se_{15}$. $Nb_2Pd_3Se_8$ is synthesized from the $Pd_{17}Se_{15}$ at these higher temperatures. X-ray diffraction (XRD) analysis revealed that the wires exhibit a preferred orientation along the (210) plane. Electronic device fabrication using these wires demonstrated their application potential as n-type semiconductors. Field-effect transistor (FET) measurements revealed remarkable performance, with an Ion/Ioff ratio of 575 and an electron mobility of 2.03 $cm^2\ V^{-1}\ s^{-1}$. LPI-CVD provides a promising strategy for synthesizing ternary chalcogenide materials, opening possibilities for exploring diverse ternary phases. This study highlights the importance of controllability, reproducibility, and FET performance in growing $Nb_2Pd_3Se_8$ wires *via* the CVD system, thereby paving the way for integrated applications and facilitating mixed-dimensional studies with other nanomaterials.

Received 7th May 2024,
Accepted 25th July 2024

DOI: 10.1039/d4ce00451e

rsc.li/crystengcomm

1. Introduction

Graphene, black phosphorus (BP), carbon nanotubes (CNTs), and other atomically thin elemental nanomaterials with 1D/2D van der Waals (vdW) bonding possess attractive physical and chemical properties.[1–3] However, challenges such as stability, chirality, and band gap limitations have been encountered. In recent decades, researchers have focused on studying binary systems, which are known as transition metal dichalcogenides (TMDCs), to address these material limitations.[4–6] Furthermore, ternary phase materials, which provide a great range of elemental combinations, have been investigated. Ternary chalcogenides exhibit diverse crystal structures because of different atomic arrangements and bonding configurations within the compounds. These variations in crystal structure result in distinct electronic structures and unique electronic properties compared with their binary counterparts. One notable example is Bi_2O_2Se, a bismuth oxychalcogenide with planar covalently bonded oxide layers (Bi_2O_2) sandwiched between Se square arrays. Bi_2O_2Se demonstrates a low in-plane electron effective mass ($m^* = 0.14$) and a Hall mobility of 450 $cm^2\ V^{-1}\ s^{-1}$ at room temperature.[7] Another family of ternary chalcogenides is metal thiophosphides (MPX_3), which exhibit a $(P_2S_6)^{4-}$ bipyramidal structure with a honeycomb arrangement of transition metal ions (Mn, Fe, Co, Ni, Zn, and Cd). These

---

[a] *School of Advanced Materials Science & Engineering, Sungkyunkwan University, Suwon 16419, Republic of Korea. E-mail: shkim407@gmail.com, jy.choi@skku.edu*
[b] *SKKU Advanced Institute of Nanotechnology (SAINT), Sungkyunkwan University, Suwon 16419, Republic of Korea*
[c] *Department of Materials Science and Engineering & Department of Energy Systems Research, Ajou University, Suwon 16499, Republic of Korea. E-mail: hakkiyu@ajou.ac.kr*
[d] *KIST-SKKU Carbon-Neutral Research Center, Sungkyunkwan University, Suwon 16419, Republic of Korea*

† Electronic supplementary information (ESI) available. See DOI: **https://doi.org/10.1039/d4ce00451e**

‡ These authors contributed equally.

materials vary in absorption edge energies, ranging from 1.5 to 3.5 eV, depending on the specific transition metal ion.[8] In addition, various ternary transition metal chalcogenides, such as Cu_2MoS_4,[9] Ta_2NiSe_5,[10] $Fe_3Ge_2Te_6$,[11] and Nb_2PdS_6,[12] have shown potential application in photocatalysis, optoelectronics, spintronics, interconnects, and energy conversion.

One of the ternary transition metal chalcogenides, $Nb_2Pd_3Se_8$, was first synthesized by Keszler *et al.* in 1984.[13] It is a 1D structure composed of combinations of metals such as Ta or Nb, as well as Ni, Pt, Pd, S, or Se, forming an $M_2N_3X_8$ structure (M = Ta or Nb, N = Ni or Pt or Pd, X = S or Se).[13–20] As shown in Fig. 1a, the transition metal is surrounded by Se atoms, and chemically stable Pd and Nb atoms form a superlattice structure in the order of Pd–Nb–Pd–Nb–Pd. This structure forms long wires in the [001] direction. The distance between the Pd atom on the outer side of the ribbon and the adjacent Se is 2.6 Å, with a binding energy of 0.39 eV per atom, like hydrogen bonding. Consequently, $Nb_2Pd_3Se_8$ is evaluated as a highly stable material that maintains its electrical properties even in ambient air for 60 days. It has an indirect band gap of 0.73 eV in bulk and a narrow band gap of 0.44 eV in a single ribbon, making it useful in the fields of optics and electronics.[15,17]

Electrical control of traditional and collective currents in 1D material systems such as $Nb_2Pd_3Se_8$ is anticipated to be highly effective due to their small cross-sectional dimensions and reduced boundary scattering resulting from self-passivated surfaces.[21] Accordingly, $Nb_2Pd_3Se_8$ grown by the chemical vapor transport (CVT) method, which is a deterministic synthesis method, was mechanically exfoliated to obtain atomic layers at the sub-nanometer level or

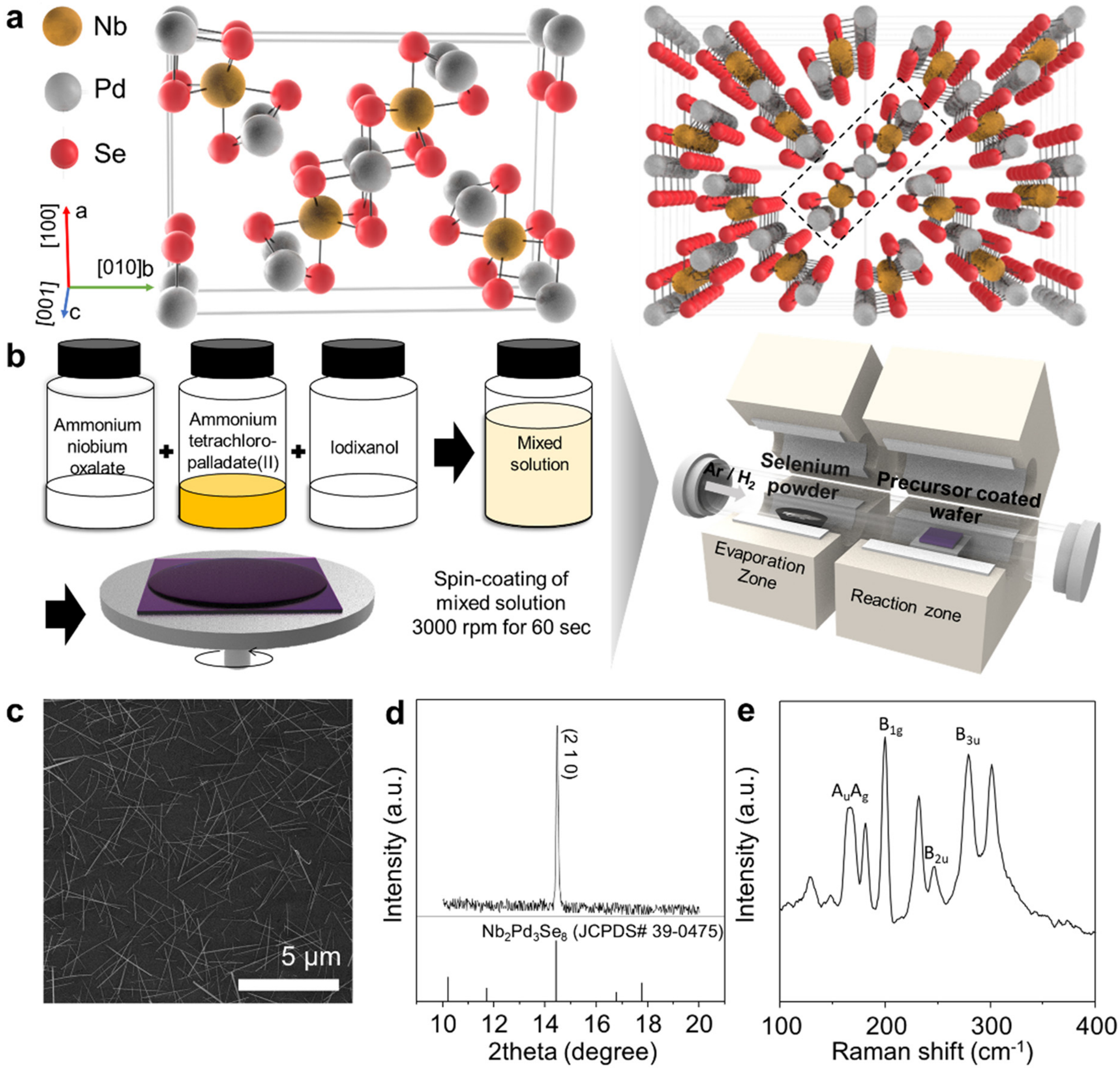

Fig. 1 $Nb_2Pd_3Se_8$ nanowire synthesized using LPI-CVD. (a) Crystal structure of the 1D $Nb_2Pd_3Se_8$. (b) Schematic illustration of the LPI-CVD process for $Nb_2Pd_3Se_8$. (c) SEM image showcasing the morphology of the synthesized nanowires. (d) XRD (e) Raman spectra of $Nb_2Pd_3Se_8$ grown on SiO_2 substrate.

separated to the 12 nm level using liquid precursor exfoliation to evaluate the intrinsic properties of the material.[20] In particular, 1D vdW materials exhibit various properties depending on the number of bonded wires and layers, and their anisotropic structure results in directional variation in properties.[17,18] Through optical studies of a recently discovered highly anisotropic structure, $Nb_2Pd_3Se_8$, in-plane optical anisotropy and anisotropic phonon vibrations have been investigated. The research demonstrated ultra-broadband detectivity and a high linear anisotropic ratio.[22] However, top-down methods have limitations such as the generation of unwanted residues, difficulty in mass transfer to substrates, and precise control of size. Therefore, precisely controlling the reaction on the substrate is necessary to manipulate such properties.

Bottom-up chemical vapor deposition (CVD) methods enable the synthesis of target materials on a large scale and allow control over the shape and performance of materials by adjusting gases and pressures. Precursor modulation enables the controlled synthesis of materials by stacking blocks atomically, utilizing the orientation and lattice mismatch between the material and substrate to control the dimension of various vdW materials.[23–25] As a counterpart to the research on two-dimensional materials, various one-dimensional materials are being investigated through diverse vapor-phase synthesis methods.[26–29] In the case of $Nb_2Pd_3Se_8$, a carrier gas containing metals is necessary to create two or more metallic precursors in a gaseous state. However, achieving uniform synthesis throughout the substrate requires precise methods.[30–32] Therefore, the CVD synthesis of the ternary phase of nanomaterials is challenging.

Thus, we focused on a method of synthesizing metal precursors at low temperatures using conventional CVD synthesis of nanomaterials.[33–37] For example, Han *et al.* successfully synthesized MoS_2 by spin casting a salt of molybdenum ammonium heptamolybdate dissolved in deionized (DI) water on a target substrate.[33] This liquid precursor-intermediated CVD (LPI-CVD) method has been further investigated with a focus on synthesizing binary TMDCs, similar to initial studies on 2D materials.

In this study, we performed CVD synthesis of $Nb_2Pd_3Se_8$ for the first time, a ternary chalcogenide 1D vdW material, using different precursors. We controlled the coating of Nb and Pd salts as precursors and successfully synthesized $Nb_2Pd_3Se_8$ wires with a thickness of 20 nm and a length of 10 μm using CVD. Reproducibility confirmed that the material $Nb_2Pd_3Se_8$ can be stably synthesized in a 1D shape, and the evaluation of electrical properties confirmed its performance as a 1D n-type semiconductor.

Therefore, synthesizing ternary systems beyond the current binary system demonstrates the potential for further research on various ternary phases. Furthermore, the CVD synthesis of 1D vdW material with semiconductor properties can serve as a basis for integrated applications using nanomaterials and provide solutions applicable to mixed-dimensional studies with various dimensions in the future.[38–40]

2. Experimental sections

2.1 Growth of $Nb_2Pd_3Se_8$

An aqueous precursor solution was prepared for the growth of $Nb_2Pd_3Se_8$, which consists of a mixed solution of aqueous ammonium niobium oxalate ($C_4H_4NNbO_9 \cdot xH_2O$, Sigma-Aldrich), aqueous ammonium tetrachloropalladate ($(NH_4)_2PdCl_4$, Sigma-Aldrich), and OptiPrep density gradient medium (Iodixanol, Sigma-Aldrich) with volume ratio 4 : 4 : 1. The liquid precursor was mixed in a 2 : 3 molar ratio of Nb (40 mM) : Pd (60 mM) using a micropipette. Substrates were sonicated in acetone, ethanol and DI water and they were cleaned with O_2 plasma (30 W, 3 min) to improve wettability. And then 400 μl of liquid precursor was dropped onto the SiO_2 substrate (2 × 2 cm) and then spin coated at 3000 rpm for 30 s and then pre-bake at 120 °C for 30 min on the hot plates.

The carbon residues on samples were removed by calcinating at 600 °C with a ramp rate of 20 °C min^{-1} for 3 h in a box furnace under ambient conditions. Subsequently, the precursor coated substrate was placed in the center of the reaction zone, and 1 g of selenium powder was loaded in 5 ml alumina boat in the evaporation zone. (Fig. 2b) The furnace was heated to the desired temperatures (620–730 °C) for 5 min with 450 sccm of argon gas and 20 sccm of hydrogen gas and maintained for 40 min. After the reaction finished, the furnace was naturally cooled. Schematic diagram of the $Nb_2Pd_3Se_8$ nanowire is demonstrated in Fig. S1.†

2.2 Characterization and device fabrication

Material characterization. X-ray Diffraction (XRD; D8 Advance, Bruker) was performed using Cu K_α radiation (λ = 0.154 nm) at a scanning rate of 2° min^{-1}.

Morphological analysis was conducted using field-emission scanning electron microscopy (FE-SEM; Hitachi, S-4300SE) at an accelerating voltage of 15 kV and a beam current of 10 μA.

All topographic analyses were performed in tapping mode using a Park system with Si cantilevers (≈300 kHz resonant frequency) coated with Al (Tap300 Al, Budget Sensors Inc.) at a scanning rate of ≈0.4 Hz. Aberration-corrected scanning transmission electron microscopy (STEM; JEOL, JEM-ARM200F) was performed at an acceleration voltage of 200 kV. Raman spectroscopy (LabRAM HR Evolution, HORIBA) was used to define the vibration modes of materials using a 785 nm laser.

Device fabrication. Field-effect transistor (FET) device was fabricated by standard photolithography method in which the photoresist AZ512E was spin-coated onto as prepared substrate at 4000 rpm and pre-baked at 110 °C for 1 min on a hotplate, and then it was exposed to ultra-violet light to define the source/drain electrodes. After exposure, it was developed using developer AZ300MIF and Cr/Au (5/100 nm)

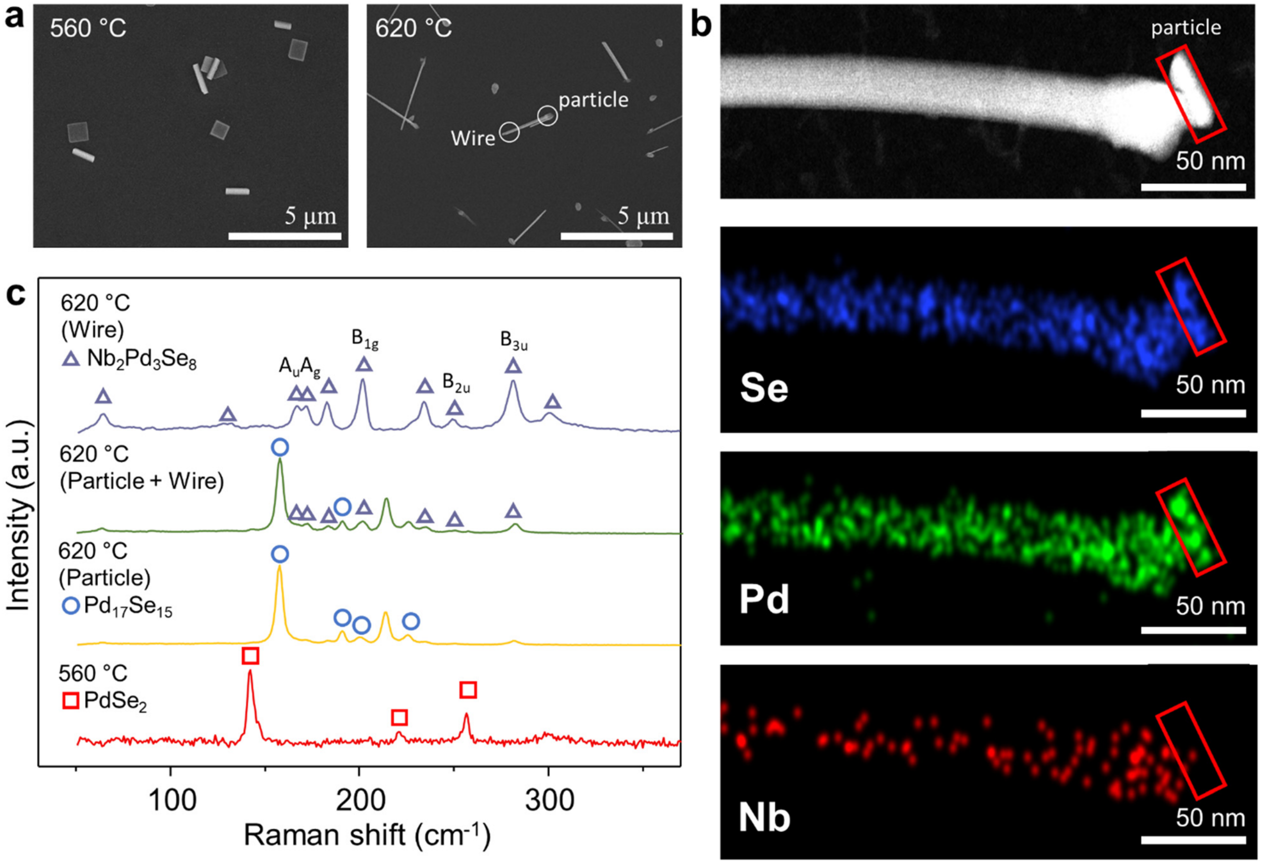

Fig. 2 Growth of $Nb_2Pd_3Se_8$ on SiO_2. (a) SEM images of $Nb_2Pd_3Se_8$ as grown at 560 and 620 °C (b) STEM-EDS mapping of $Nb_2Pd_3Se_8$ grown at 620 °C, with the inset red rectangle highlighting the particle of $Nb_2Pd_3Se_8$ (c) Raman spectra of grown at 560 and 620 °C.

were deposited by e-beam evaporation under high vacuum conditions (5×10^{-7} torr).

Charge transport measurements. Electrical measurement of $Nb_2Pd_3Se_8$ transistors was performed in vacuum (below 1×10^{-3} torr) conditions in an M6VC probe station with different temperatures. Three Keithley source meter 4200 SCS units were used to measure the transfer characteristics.

3. Results and discussion

An aqueous precursor solution was prepared for the growth of $Nb_2Pd_3Se_8$, which consists of a mixed solution of aqueous ammonium niobium oxalate (niobium precursor), aqueous ammonium tetrachloropalladate(II) (palladium precursor), and iodixanol. The precursor was mixed in a 2 : 3 molar ratio of Nb : Pd using a micropipette. The prepared precursor solution was coated on SiO_2 using a spin coater, and calcination was performed. Fig. S2† illustrates the morphology of the precursors deposited on the substrate after calcination, showing uniformly deposited particles of approximately 10 nm in size. The number of particles increased with precursor concentration, indicating the controllability of the precursor. Subsequently, the substrate with the coated precursor was placed in an atmosphere-pressure CVD system, and Se was supplied during the experiment (Fig. 1b). As shown in Fig. 1c, $Nb_2Pd_3Se_8$ wires were grown randomly on the substrate. Ribbon-shaped particles, as observed in the lattice structure, were arranged in a zigzag pattern, and each ribbon was formed in a tilted structure close to the (210) plane of the lattice.[16,17] The $Nb_2Pd_3Se_8$ grown on the substrate exhibited a strong preference peak at 14.43°, corresponding to the (210) plane of $Nb_2Pd_3Se_8$ as observed through X-ray diffraction (Fig. 1d). According to the Wulff theorem, the shape of nanocrystals is determined by the surface energy of their crystallographic facets.[41] This preferred peak can be attributed to the structural characteristics of the material. This preference is also seen in $Nb_2Pd_3Se_8$ growth on the substrate. During the thermodynamic growth of nuclei, nanocrystals tend to grow faster on high-energy facets. For $Nb_2Pd_3Se_8$, the (210) facet, like $Ta_2Pd_3Se_8$, has high surface energy, resulting in faster growth rates along this facet, which manifests as the preferential appearance in PXRD.[25] Therefore, the wires grow perpendicular to the substrate along the (210) facet, as shown in Fig. S3.† The SEM image illustrates nanowires growing attached to the substrate. (Fig. S3†) Raman spectroscopy revealed peaks at 166.7 (A_u), 171.6 (A_g), 202.2 (B_{1g}), 250.4 (B_{2u}), and 301.2 (B_{3u}) cm^{-1}, which are similar to the calculated values for $Nb_2Pd_3Se_8$ (Fig. 1e).[19]

In the CVD system, $NbSe_2$ was synthesized at 800–850 °C.[42,43] On the contrary, $PdSe_2$ was synthesized between 300 and 550 °C.[44,45] $Nb_2Pd_3Se_8$ was synthesized at intermediate temperatures ranging from 600 to 800 °C in solid-state synthesis.[13,17] In this experiment, synthesis was conducted in the CVD system at a temperature range of 570 to 730 °C, which is between the synthesis temperatures of $PdSe_2$ and $NbSe_2$. As shown in Fig. 2a and S4,† plate-shaped $PdSe_2$ was synthesized at 570 °C, and wire formation was observed at 620 °C in some of the particles. Electron dispersion spectroscopy (EDS) mapping of the wires was performed to investigate the particle portion of the wires synthesized at 620 °C (Fig. 2b). The scanning transmission electron microscopy (STEM) EDS mapping data confirmed the presence of Nb, Pd, and Se compositions in the wires, whereas only Pd and Se compositions were observed in the particle portion. As shown in Fig. 2c, the nanoplates synthesized at 570 °C exhibited peaks at 145, 208, and 260 cm^{-1}, corresponding to $PdSe_2$.[45–48] In the particle portion synthesized at 620 °C, Raman peaks at 157.7, 190, 213.5, and 226.3 cm^{-1}, corresponding to $Pd_{17}Se_{15}$,[48] were formed, whereas the wire portion showed peaks at 166.70, 171.5, 202.48, 250.35, and 301.2 cm^{-1}, corresponding to $Nb_2Pd_3Se_8$.[19] Based on these Raman peaks observed, spectra simultaneously present in both the wire ($Nb_2Pd_3Se_8$) and particle ($Pd_{17}Se_{15}$) portions suggest that these particles act as seeding promoters for $Nb_2Pd_3Se_8$.

Experiments were conducted at 560, 580, 600, and 620 °C to determine the synthesis temperature of $Nb_2Pd_3Se_8$ wires. Fig. 3a shows the temperature profile, where the temperature of the evaporation zone for the supply of Se was kept constant while the process temperature varied (experimental temperature was designed based on the phase diagram of Pd–Se shown in Fig. 3b). Fig. 3c displays SEM images corresponding to different synthesis temperatures. At 600 °C, only $PdSe_2$ was formed, and $Nb_2Pd_3Se_8$ did not synthesize. At 560, 580, and 600 °C, square-shaped $PdSe_2$ was observed. At 620 °C, $PdSe_2$ was not observed, and the growth of $Nb_2Pd_3Se_8$ wires from $Pd_{17}Se_{15}$ was observed. As shown in phase diagram (Fig. 3b), the cause of this behaviour can be explained as follows: as the process temperature increases, the phase transition from $PdSe_2$ to $Pd_{17}Se_{15}$ is induced during heating.[47,48] Excessive Se, released during phase transition, contributes to the synthesis of $Nb_2Pd_3Se_8$ wires.

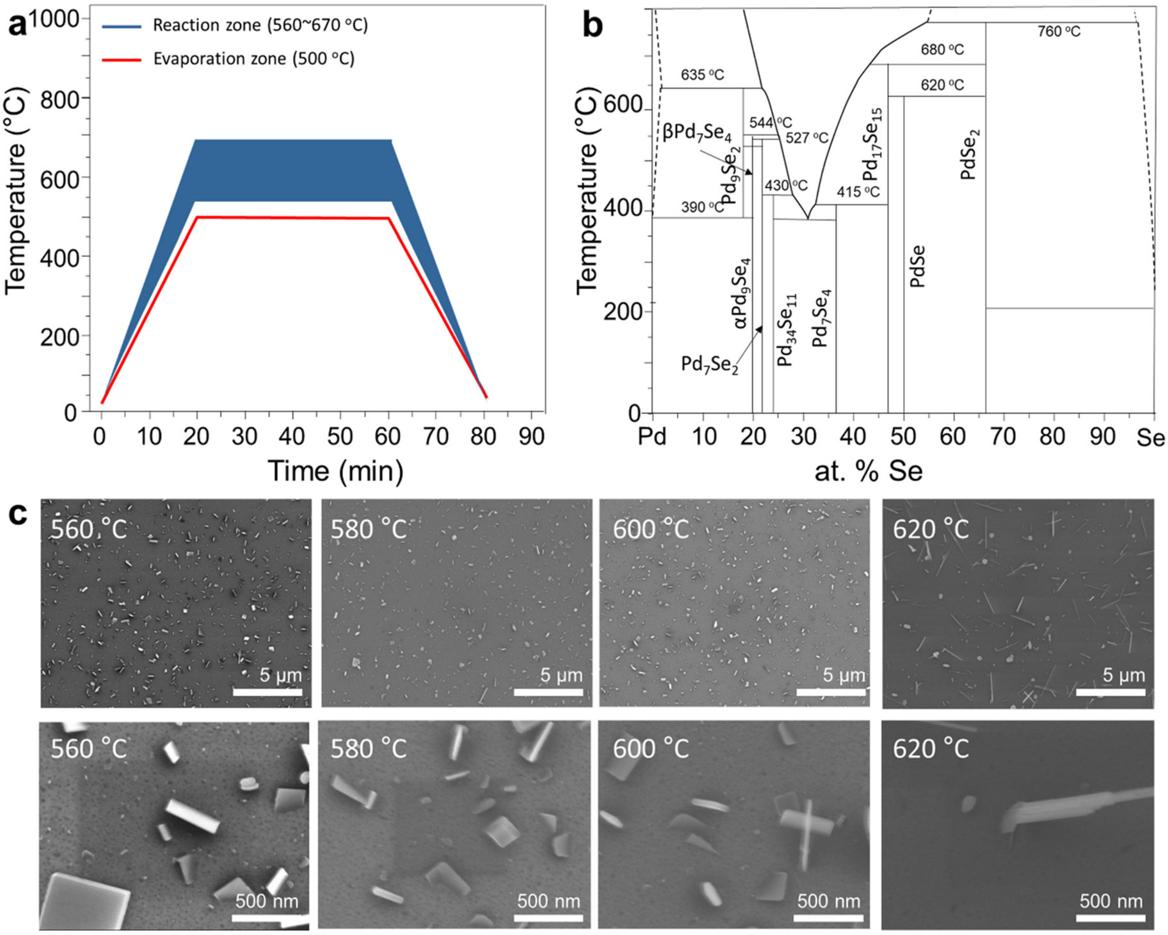

Fig. 3 Effect of LPI-CVD process temperatures on synthesis. (a) Temperature profile of CVD synthesis. (b) Phase diagram illustrating the Pd–Se binary alloy system. (c) SEM images after the LPI-CVD process at temperatures 560, 580, 600 and 620 °C.

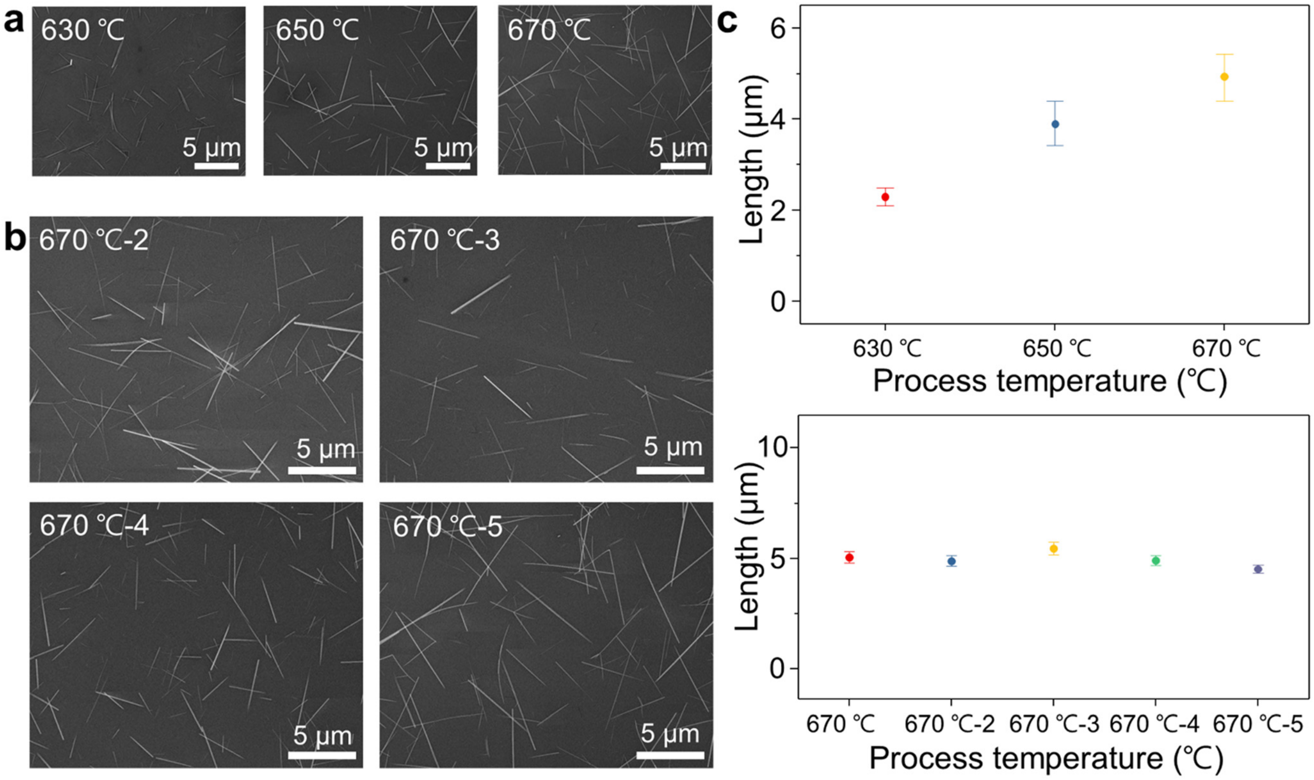

Fig. 4 Growth of $Nb_2Pd_3Se_8$ with various process temperatures. (a) SEM images of $Nb_2Pd_3Se_8$ grown at 630, 650 and 670 °C. (b) Repetition results at 670 °C for four times. (c) Wire length dependent on process temperatures (top) and repetition experiments (bottom).

Fig. 4a and b displays SEM images showing the synthesis of $Nb_2Pd_3Se_8$ wires at different temperatures. The average lengths of the synthesized $Nb_2Pd_3Se_8$ wires at 630, 650, and 670 °C are 2.29, 3.91, and 4.91 μm, respectively. In confirming reproducibility, four additional experiments were conducted at 670 °C, yielding wire lengths of 5.18, 4.89, 5.28, 4.91, and 4.53 μm. Length variations with temperature and the reproducibility results are presented in the histogram shown in Fig. 4c. At 690, 710, and 730 °C, $Nb_2Pd_3Se_8$ wires were synthesized with average lengths of 11.55, 15.04, and 13.88 μm, respectively, and as a result, the aspect ratio was calculated with the increasing of process temperature. (See the ESI† Fig. S5). As shown in Pd–Se phase diagram (Fig. 3b), at temperatures above 680 °C, the $Pd_{17}Se_{15}$ phase cannot exist, and the observed growth was attributed to the partial growth in the liquid Se phase resulting from the rapid decomposition of $PdSe_2$.[47] However, at high process temperatures, a red shift was observed in the Raman spectra. Doped $Nb_2Pd_3Se_8$ exhibited a red shift of 0.8 cm^{-1} compared with doped $AuCl_3$ in previous research,[19] whereas the B_{1g} peak observed at 670, 690, and 710 °C showed significant shifts of 199.3, 197.7, and 195.29 cm^{-1}, respectively (see the ESI† Fig. S6). This phenomenon is due to the loss of outermost Se atoms as shown in the thermogravimetric analysis (TGA) data above 480 °C.[17] After processing at 650 °C, the loss of Se atoms from the outer region contributes to this phenomenon.

STEM study was conducted on the synthesized $Nb_2Pd_3Se_8$. The selected area electron diffraction (SAED) pattern shown in Fig. 5a indicates that the as synthesized wire is a single crystalline. High-resolution ADF-STEM images shown in Fig. 5b and c reveal the growth direction of the wire, which aligns with the (001) plane of $Nb_2Pd_3Se_8$, corresponding to the chain direction. Furthermore, the outer direction of the wire corresponds to the (110) plane, with a distance of 8.87 Å.[20] Fig. 5d presents the EDS results obtained through STEM analysis, showing the presence of Nb, Pd, and Se. The Nb : Pd : Se ratio is determined to be 2 : 3.08 : 7.54, indicating Se deficiency. Moreover, the chemical bonding characteristics of $Nb_2Pd_3Se_8$ nanowires were verified using X-ray photoelectron spectroscopy (XPS) in Fig. S6.† The XPS of $Nb_2Pd_3Se_8$ grown on the substrate was examined. The binding energies for Nb 3d, Pd 3d, and Se 3d in the XPS of $Nb_2Pd_3Se_8$ are as follows, the peaks observed at 204.7 and 207.4 eV correspond to Nb–Se $3d_{5/2}$ and Nb–Se $3d_{3/2}$. Peaks at 337.5 and 342.7 eV correspond to Pd $3d_{5/2}$ and Pd $3d_{3/2}$, and peaks at 54.4 and 55.2 eV correspond to Se $3d_{5/2}$ and Se $3d_{3/2}$ (Fig. S7†).[41] Higher binding energy peaks of Nb 3d binding energy indicating Nb–O $3d_{5/2}$ and Nb–O $3d_{3/2}$ were detected, suggesting the presence of unreacted niobium oxide. The extracted atomic percentages for these peaks, excluding the niobium oxide energy peaks, align well with the STEM-EDS data ratios, with an atomic ratio of Nb/Pd/Se being 15.77 : 24.50 : 59.70 (2 : 3.10 : 7.56). This consistency supports the observed Se deficiency in the Nb2Pd3Se8 nanowires. This

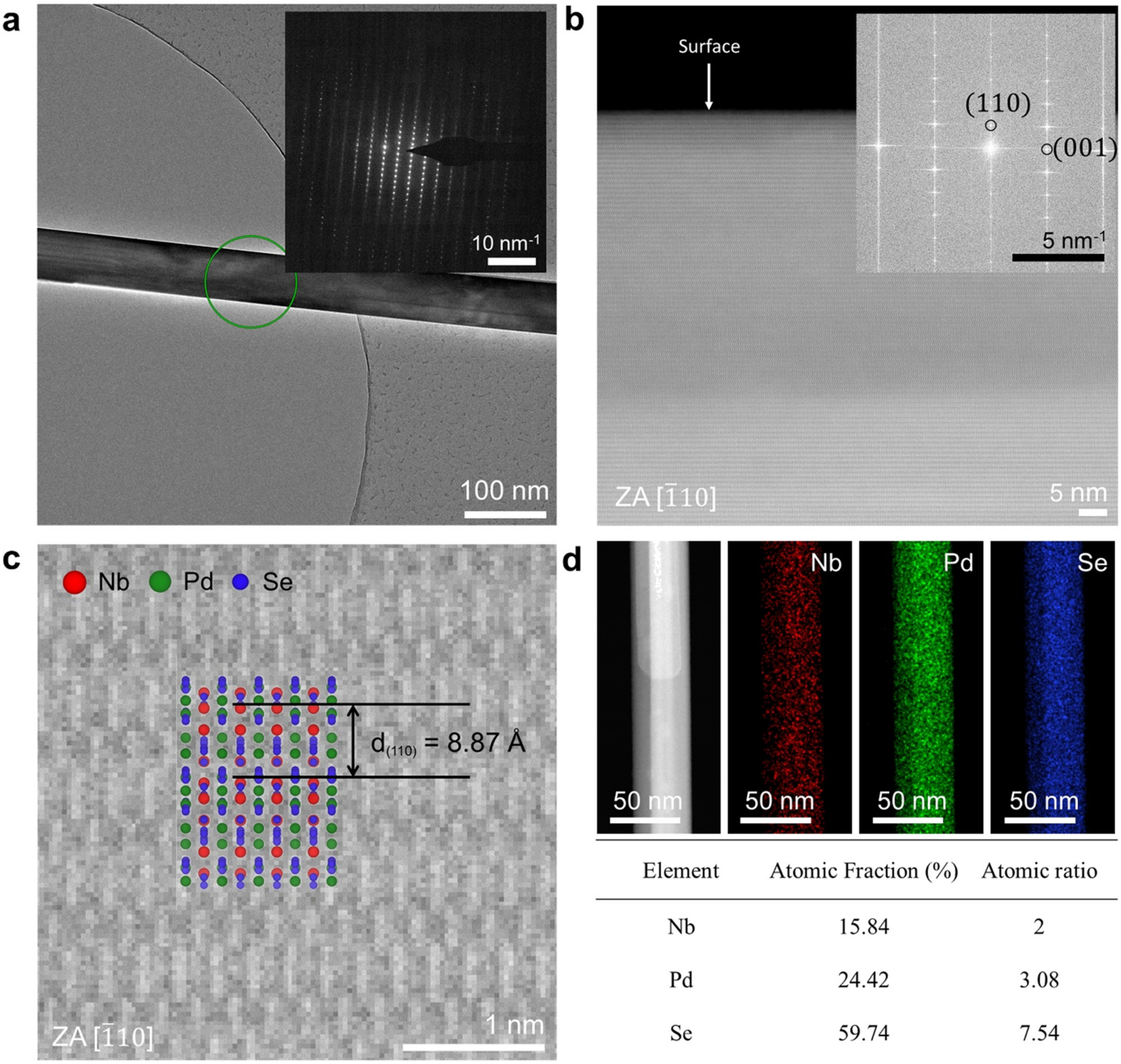

Element	Atomic Fraction (%)	Atomic ratio
Nb	15.84	2
Pd	24.42	3.08
Se	59.74	7.54

Fig. 5 STEM study. HADDF-STEM: (a) low-magnification (inset image shows the SAED pattern) and (b) high-magnification image of $Nb_2Pd_3Se_8$ (inset image shows the FFT pattern) (c) STEM images with zone axis [110] (d) EDS mapping data of $Nb_2Pd_3Se_8$.

finding is consistent with Se deficiency observed in the TGA results of $Nb_2Pd_3Se_8$, indicating the loss of Se after synthesis.

A device shown in Fig. 6a was fabricated at a CVD process temperature of 630 °C to assess the quality of the synthesized $Nb_2Pd_3Se_8$ for electronic devices. The FET device was produced by depositing Ti/Au on the CVD-grown $Nb_2Pd_3Se_8$ using photolithography. In addition, the dimension of $Nb_2Pd_3Se_8$ among the devices was examined using SEM and AFM (Fig. 6b and S8†). Fig. 6c presents the output curves (I_{ds}–V_{ds}) from −20 to 40 V, indicating the characteristics of an n-type semiconductor. In verifying the FET effect, transfer curves were measured by applying gate voltages (V_{gs}) ranging from −50 to 50 V at room temperature. The measured Ion/Ioff ratio was 575, and the threshold voltage was observed at −20 V. The field-effect mobility was calculated using the following formula;

$$\mu_{FE} = \left(\frac{L}{WC_{ox}V_{ds}}\right)\left(\frac{\partial I_{ds}}{\partial V_g}\right),$$

where the parameters L, W, and C_{ox} are the channel length, channel width, and capacitance of the 100 nm SiO_2 dielectric layer per unit area. The calculated electron mobility of this specific device was 2.03 cm^2 V^{-1} s^{-1}.

4. Conclusions

In conclusion, we successfully synthesized $Nb_2Pd_3Se_8$ wires, a ternary chalcogenide 1D van der Waals material, *via* liquid-phase intermediated chemical vapor deposition (LPI-CVD). By controlling the coating of Nb and Pd salts as precursors, we achieved the synthesis of $Nb_2Pd_3Se_8$ wires with reproducible

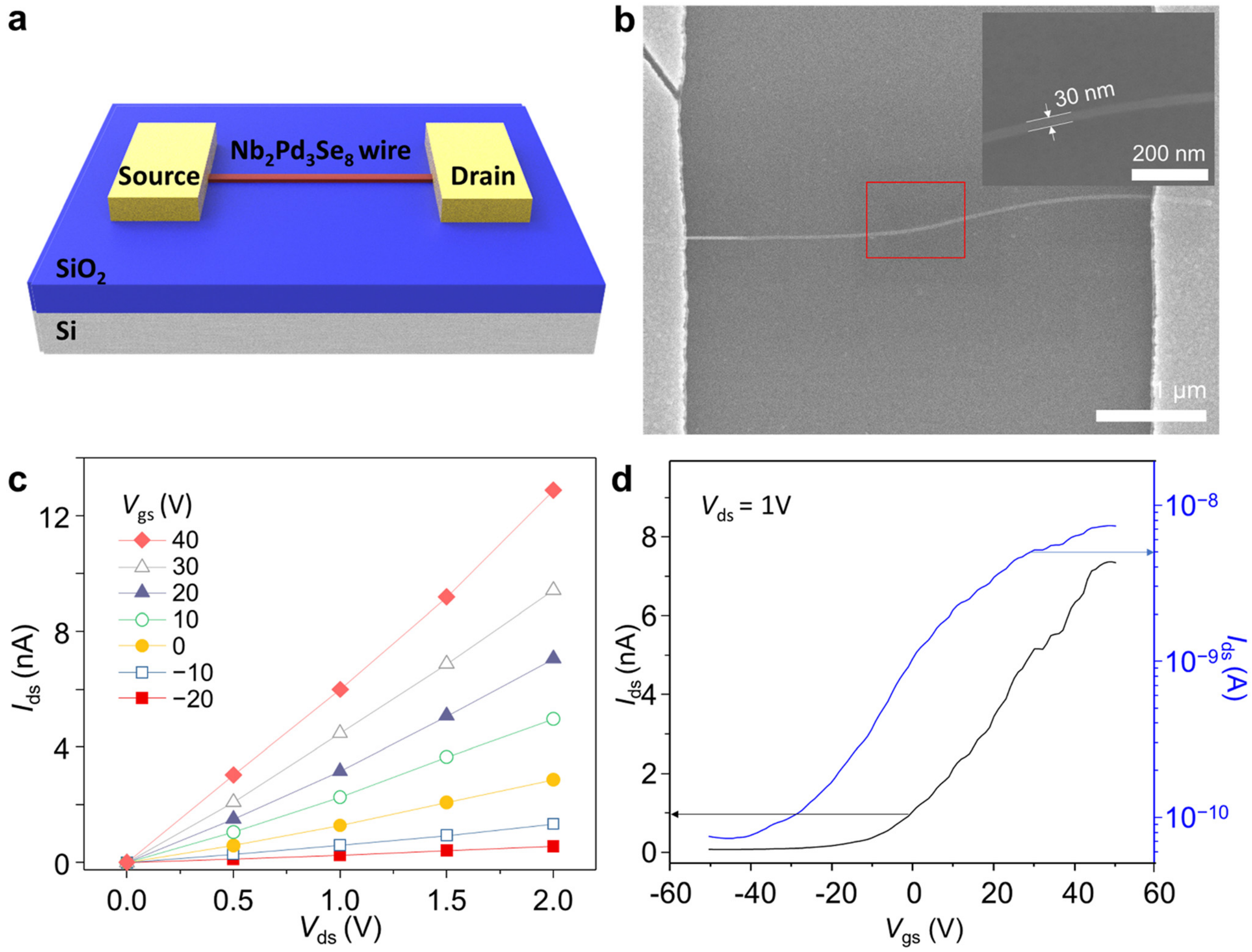

Fig. 6 FET property of LPI-CVD-grown $Nb_2Pd_3Se_8$. (a) Schematic of the $Nb_2Pd_3Se_8$ electronic device. (b) SEM images of the device. Inset is the enlarged photo of the red bordered square area. (c) RT output characteristic (I_{ds}–V_{ds}) of $Nb_2Pd_3Se_8$ FET under a gate bias ranging from −20 to 40 V. (d) RT transfer characteristic (I_{ds}–V_{gs}) of $Nb_2Pd_3Se_8$ FET under V_{ds} of 1 V.

dimensions and electrical properties. Our results demonstrate the feasibility of synthesizing ternary systems beyond binary systems, indicating avenues for further exploration in diverse ternary phases. Moreover, the CVD synthesis of 1D van der Waals materials with semiconductor properties holds promise for integrated applications in nanomaterials and offers solutions applicable to mixed-dimensional studies. The characterization of $Nb_2Pd_3Se_8$ wires through electron microscopy, spectroscopy, and device fabrication underscores its potential for electronic applications, as evidenced by the observed field-effect transistor behaviour and calculated electron mobility. Overall, our study contributes to the understanding and utilization of ternary chalcogenides in the realm of nanomaterials and electronics.

Data availability

The data that support the findings of this study are available from the corresponding author, upon reasonable request.

Author contributions

S. H. L. and B. J. J. contributed equally to this work. S. H. L. and B. J. J. were responsible for conceptualization, investigation, methodology, and writing – original draft. K. H. C., J. J., D. K., G. T. G., D. D. M. supported the analysis and investigation. S. C., B. L. and supported FET measurement. S. H. K., J. -Y. C. and H. K. Y. supervised the whole project.

Conflicts of interest

There are no conflicts to declare.

Acknowledgements

This research was supported by the Basic Science Research Program through the National Research Foundation of Korea, funded by the Korean government (MSIT, RS-2023-00208311). In addition, this work was supported by the KIST Institutional

Program (Project No. 2E31854-22-066) from the Korea Institute of Science and Technology.

References

1 K. S. Novoselov, A. K. Geim, S. V. Morozov, D. Jiang, M. I. Katsnelson, I. V. Grigorieva, S. Dubonos and A. Firsov, *Nature*, 2005, **438**, 197–200.

2 F. Xia, H. Wang and Y. Jia, *Nat. Commun.*, 2014, **5**, 4458.

3 S. Iijima and T. Ichihashi, *Nature*, 1993, **363**, 603–605.

4 B. Radisavljevic, A. Radenovic, J. Brivio, V. Giacometti and A. Kis, *Nat. Nanotechnol.*, 2011, **6**, 147–150.

5 K. F. Mak, C. Lee, J. Hone, J. Shan and T. F. Heinz, *Phys. Rev. Lett.*, 2010, **105**, 136805.

6 W. Liu, J. Kang, D. Sarkar, Y. Khatami, D. Jena and K. Banerjee, *Nano Lett.*, 2013, **13**, 1983–1990.

7 J. Wu, H. Yuan, M. Meng, C. Chen, Y. Sun, Z. Chen, W. Dang, C. Tan, Y. Liu and J. Yin, *Nat. Nanotechnol.*, 2017, **12**, 530–534.

8 Q. Liang, Y. Zheng, C. Du, Y. Luo, J. Zhang, B. Li, Y. Zong and Q. Yan, *Small Methods*, 2017, **1**, 1700304.

9 W. Chen, H. Chen, H. Zhu, Q. Gao, J. Luo, Y. Wang, S. Zhang, K. Zhang, C. Wang and Y. Xiong, *Small*, 2014, **10**, 4637–4644.

10 Y. Lu, H. Kono, T. Larkin, A. Rost, T. Takayama, A. Boris, B. Keimer and H. Takagi, *Nat. Commun.*, 2017, **8**, 14408.

11 Y. Deng, Y. Yu, Y. Song, J. Zhang, N. Z. Wang, Z. Sun, Y. Yi, Y. Z. Wu, S. Wu and J. Zhu, *Nature*, 2018, **563**, 94–99.

12 S. Cho, B. J. Jeong, K. H. Choi, B. Lee, J. Jeon, S. H. Lee, B. J. Kim, J. H. Lee, H. S. Oh and H. K. Yu, *Small*, 2022, **18**, 2205344.

13 D. A. Keszler and J. A. Ibers, *J. Solid State Chem.*, 1984, **52**, 73–79.

14 K. H. Choi, B. J. Jeong, J. Jeon, Y. K. Chung, D. Sung, S. O. Yoon, S. Chae, B. J. Kim, S. Oh and S. H. Lee, *Small*, 2021, **17**, 2102602.

15 B. J. Jeong, K. H. Choi, J. Jeon, S. O. Yoon, Y. K. Chung, D. Sung, S. Chae, S. Oh, B. J. Kim and S. H. Lee, *Nanoscale*, 2021, **13**, 17945–17952.

16 Q. Zhang, C. Liu, X. Liu, J. Liu, Z. Cui, Y. Zhang, L. Yang, Y. Zhao, T. T. Xu and Y. Chen, *ACS Nano*, 2018, **12**, 2634–2642.

17 B. J. Jeong, K. H. Choi, J. Jeon, S. O. Yoon, Y. K. Chung, D. Sung, S. Chae, B. J. Kim, S. Oh and S. H. Lee, *Adv. Funct. Mater.*, 2022, **32**, 2108104.

18 M. Luo, T. Wu, S. Xu, R. Wang and F. Huang, *Chem. Commun.*, 2022, **58**, 6204–6207.

19 B. J. Jeong, B. Lee, K. H. Choi, D. Sung, S. Ghods, J. Lee, J. Jeon, S. Cho, S. H. Lee and B. J. Kim, *Nano Lett.*, 2023, **23**, 6269–6275.

20 K. H. Choi, J. Jeon, B. J. Jeong, S. Chae, S. Oh, C. Woo, T. Y. Kim, J. Ahn, J. H. Lee and H. K. Yu, *Adv. Mater. Interfaces*, 2022, **9**, 2200620.

21 A. A. Balandin, F. Kargar, T. T. Salguero and R. K. Lake, *Mater. Today*, 2022, **55**, 74–91.

22 Q. Qin, W. Gao, H. Zhang, J. Chen, Y. Yan, K. Zhu, M. Long, G. Li, S. Yin and Y. Du, *J. Mater. Chem. A*, 2023, **11**, 11517–11525.

23 P. Yang, S. Zhang, S. Pan, B. Tang, Y. Liang, X. Zhao, Z. Zhang, J. Shi, Y. Huan and Y. Shi, *ACS Nano*, 2020, **14**, 5036–5045.

24 Z. Ma, S. Wang, Q. Deng, Z. Hou, X. Zhou, X. Li, F. Cui, H. Si, T. Zhai and H. Xu, *Small*, 2020, **16**, 2000596.

25 Q. Zhang, X. Xiao, L. Li, D. Geng, W. Chen and W. Hu, *Small*, 2022, **18**, 2107241.

26 R. Natsui, H. Shimizu, Y. Nakanishi, Z. Liu, A. Shimamura, N. T. Hung, Y.-C. Lin, T. Endo, J. Pu and I. Kikuchi, *ACS Nano*, 2023, **17**, 5561–5569.

27 M. Sun, J. Li, Q. Ji, Y. Lin, J. Wang, C. Su, M.-H. Chiu, Y. Sun, H. Si and T. Palacios, *Phys. Rev. Mater.*, 2021, **5**, 094002.

28 H. E. Lim, Y. Nakanishi, Z. Liu, J. Pu, M. Maruyama, T. Endo, C. Ando, H. Shimizu, K. Yanagi and S. Okada, *Nano Lett.*, 2020, **21**, 243–249.

29 Y. Yoo, J. S. Jeong, R. Ma, S. J. Koester and J. E. Johns, *Chem. Mater.*, 2020, **32**, 9650–9655.

30 J. Zhang, F. Wang, V. B. Shenoy, M. Tang and J. Lou, *Mater. Today*, 2020, **40**, 132–139.

31 X. Ling, Y.-H. Lee, Y. Lin, W. Fang, L. Yu, M. S. Dresselhaus and J. Kong, *Nano Lett.*, 2014, **14**, 464–472.

32 L. Tang, T. Li, Y. Luo, S. Feng, Z. Cai, H. Zhang, B. Liu and H.-M. Cheng, *ACS Nano*, 2020, **14**, 4646–4653.

33 G. H. Han, N. J. Kybert, C. H. Naylor, B. S. Lee, J. Ping, J. H. Park, J. Kang, S. Y. Lee, Y. H. Lee and R. Agarwal, *Nat. Commun.*, 2015, **6**, 6128.

34 J. Seo, J. Kim, J. Lee, D. Koo, G. Jeong, Y. Choi, E. B. Son and H. Park, *Adv. Funct. Mater.*, 2022, **32**, 2205695.

35 M. Kim, J. Seo, J. Kim, J. S. Moon, J. Lee, J.-H. Kim, J. Kang and H. Park, *ACS Nano*, 2021, **15**, 3038–3046.

36 D. Jiang, X. Wang, R. Chen, J. Sun, H. Kang, D. Ji, Y. Liu and D. Wei, *J. Am. Chem. Soc.*, 2022, **144**, 8746–8755.

37 Q. Ji, C. Su, N. Mao, X. Tian, J.-C. Idrobo, J. Miao, W. A. Tisdale, A. Zettl, J. Li and J. Kong, *Sci. Adv.*, 2021, **7**, eabj3274.

38 J.-J. Tao, J. Jiang, S.-N. Zhao, Y. Zhang, X.-X. Li, X. Fang, P. Wang, W. Hu, Y. H. Lee and H.-L. Lu, *ACS Nano*, 2021, **15**, 3241–3250.

39 W. Wang, Y. Meng, W. Wang, Z. Zhang, P. Xie, Z. Lai, X. Bu, Y. Li, C. Liu and Z. Yang, *Adv. Funct. Mater.*, 2022, **32**, 2203003.

40 H. Kim, Y. C. Kim, Y. H. Ahn and Y. Yoo, *Chem. Eng. J.*, 2023, **468**, 143678.

41 A. Giri, G. Park and U. Jeong, *Chem. Rev.*, 2023, **123**, 3329–3442.

42 S. Park, S. J. Yun, Y. I. Kim, J. H. Kim, Y.-M. Kim, K. K. Kim and Y. H. Lee, *ACS Nano*, 2020, **14**, 8784–8792.

43 H. Wang, X. Huang, J. Lin, J. Cui, Y. Chen, C. Zhu, F. Liu, Q. Zeng, J. Zhou and P. Yu, *Nat. Commun.*, 2017, **8**, 394.

44 Y. Gu, H. Cai, J. Dong, Y. Yu, A. N. Hoffman, C. Liu, A. D. Oyedele, Y. C. Lin, Z. Ge and A. A. Puretzky, *Adv. Mater.*, 2020, **32**, 1906238.

45 L.-S. Lu, G.-H. Chen, H.-Y. Cheng, C.-P. Chuu, K.-C. Lu, C.-H. Chen, M.-Y. Lu, T.-H. Chuang, D.-H. Wei and W.-C. Chueh, *ACS Nano*, 2020, **14**, 4963–4972.

46 A. A. Puretzky, A. D. Oyedele, K. Xiao, A. V. Haglund, B. G. Sumpter, D. Mandrus, D. B. Geohegan and L. Liang, *2D Mater.*, 2018, **5**, 035016.

47 A. D. Oyedele, S. Yang, T. Feng, A. V. Haglund, Y. Gu, A. A. Puretzky, D. Briggs, C. M. Rouleau, M. F. Chisholm and R. R. Unocic, *J. Am. Chem. Soc.*, 2019, **141**, 8928–8936.

48 K. Ibrahim, K. C. Matthews, M. Coupin and J. H. Warner, *Chem. Mater.*, 2022, **34**, 9982–9988.